Available online at www.sciencedirect.com

SCIENCE DIRECT®

Journal of Volcanology and Geothermal Research 128 (2003) 187–199

Journal of volcanology and geothermal research

www.elsevier.com/locate/jvolgeores

The effects of a decompression on seismic parameter profiles in a gas-charged magma

Susan Sturton *, Jürgen Neuberg

School of Earth Sciences, The University of Leeds, Leeds LS2 9JT, UK

Received 18 June 2002; accepted 20 August 2002

Abstract

Seismic velocities in a gas-charged magma vary with depth and time. Relationships between pressure, density, exsolved gas content, and seismic velocity are derived and used in conjunction with expressions describing diffusive bubble growth to find a series of velocity profiles which depend on time. An equilibrium solution is obtained by considering a column of magma in which the gas distribution corresponds to the magmastatic pressure profile with depth. Decompression events of various sizes are simulated, and the resulting disequilibrium between the gas pressure and magmastatic pressure leads to bubble growth and therefore to a change of seismic velocity and density with time. Bubble growth stops when the system reaches a new equilibrium. The corresponding volume increase is accommodated by accelerating the magma column upwards and an extrusion of lava. A timescale for the system to return to equilibrium can be obtained. The effect of changes in magma viscosity and bubble number density is examined.

1. Introduction

Observations from Soufrière Hills volcano, Montserrat, and many other volcanoes show that low-frequency seismic events are important tools for assessing volcanic activity. They occur in swarms before volcanic eruptions and correlate well with tilt signals (Voight et al., 1998). Single events merge into harmonic tremor with peaked spectral amplitudes (Fehler, 1983; Neuberg et al., 1998) showing a fundamental frequency and a varying number of integer harmonics. Peaked spectra of this kind can be formed in two ways:

(1) The repetitive triggering of an identical source wavelet. The fundamental frequency and harmonics are controlled by the rate of triggering of the wavelet (Schlindwein et al., 1995; Powell and Neuberg, 2002).

(2) Eigenfrequencies of a resonating system (Benoit and McNutt, 1997).

The frequencies are sometimes seen to shift during an episode of tremor giving rise to gliding lines in spectrograms of the episodes (Neuberg, 2000). In the case of repetitive triggering, an increase in the fundamental frequency is the result of more rapid retriggering of the event. In the second case, a shift in frequency is the result of a change in the parameters controlling the oscillation of the system.

The low-frequency content of the seismic sig-

* Corresponding author. Fax: +44-113-343-5259.
E-mail address: s.sturton@earth.leeds.ac.uk (S. Sturton).

0377-0273/03/$ – see front matter © 2003 Elsevier B.V. All rights reserved.
doi:10.1016/S0377-0273(03)00254-3

nals suggests that the events are generated as interface waves at the fluid–solid boundary of a conduit filled with fluid and embedded in a solid medium. Such waves can form if the width of the conduit is narrow compared with the seismic wavelength. The characteristics of this resonating system are controlled by the ratios of the seismic wavelength to the width of the conduit and the impedance contrast between seismic parameters across the conduit wall (Biot, 1952; Chouet, 1986; Ferrazzini and Aki, 1987). In these models the frequency of oscillation would shift if there were a change in the width of the conduit, or a change in the seismic parameters inside or outside the conduit. The gliding lines are seen on timescales of minutes to hours. This means that changes in the geometry of the conduit or seismic parameters in the country rock are unlikely. However, changes in the seismic parameters of the magma are possible on this timescale.

Magmas contain a gaseous phase, and the amount of gas that is exsolved depends on the pressure. As the pressure decreases, gas dissolved in the melt will be exsolved and form bubbles. If there is a decompression caused by a dome collapse or degassing, the size of the bubbles will increase by diffusion and decompressional expansion. The gas already out of solution responds to the decrease in pressure by expanding, further increasing the volume of gas. Magma containing exsolved gas has a lower density and a dramatically lower seismic velocity (Neuberg and O'Gorman, 2002) than bubble-free magma.

Neuberg and O'Gorman (2002) show that a decrease in excess pressure will result in a change of the frequency of the resonance observed, due to an increase in the volume fraction of gas. The depth at which gas bubbles nucleate is considered to be a seismic interface in the conduit (Neuberg, 2000). When the dome collapses, the decrease in pressure results in gas exsolution deeper in the conduit. The interface therefore travels deeper into the conduit, lengthening the part of the conduit that shows a high impedance contrast with respect to the surrounding country rock. This changes the seismic wavefield. The nucleation depth is controlled by the initial gas content of the magma and the excess pressure (Neuberg, 2000), so these are important parameters in determining how much the frequency changes. The effect of changes in the initial gas content are not modelled in this paper.

Neuberg and O'Gorman (2002) model the change in excess pressure as a step function with the conduit adjusting to the new pressure instantaneously. However, the timescale over which the bubble growth takes place is important for modelling such time dependent behaviour as the gliding of the spectral lines. This will be examined in this paper.

Previous work on bubble growth has concentrated on bubble evolution at constant pressure (e.g. Lyakhovsky et al., 1996; Proussevitch et al., 1993) but only examining a limited number of final pressures, not continuous depth profiles. Proussevitch and Sahagian (1996) look at profiles of bubble radius and oversaturation with depth for gradual decompression at a constant rate obtaining a solution that is not time dependent. In contrast to these models, the approach presented in this paper describes time-dependent bubble growth for a continuous vertical profile. Approximate analytical solutions for time-dependent bubble growth under constant pressure, given by Navon and Lyakhovsky (1998), are employed to calculate the size of the bubbles present at any time and depth. The volume of exsolved gas is then used to find the seismic velocity and density of the magma, and how they change with time as the system adjusts to the new pressure.

The physical constants used are those for rhyolite applicable to volcanoes such as Soufrière Hills volcano, Montserrat, where the total rock composition is andesite but due to crystallisation the residual melt is more silicic (e.g. Devine et al., 1998). In this paper we consider a two-phase system of melt and gas and ignore the crystalline phase.

2. Depth and time-dependent seismic velocities

The volume of gas in a magma changes with magmastatic pressure. This pressure decreases if there is a collapse of dome material from the top of the conduit as often seen at andesitic volcanoes such as the Soufrière Hills volcano, Montserrat.

When the pressure decreases suddenly, a melt at equilibrium will become supersaturated and gas will diffuse into bubbles. The rate of bubble growth will depend on the concentration gradient between the water dissolved in the melt and the concentration of gas at the bubble wall, the length of time they are left to grow, and the rate at which the volatiles can be transferred along the gradient, which is given by the diffusivity and the density of the gas within the bubbles.

In the following we present two models for decompression: the first assumes as a starting point a magma under high pressure such that no gas is exsolved. The second model represents a partial decompression of a magma in which gas bubbles are already present.

2.1. The 'champagne bottle' model

An accelerating magma model is used to obtain the gas volume fraction and therefore the density and seismic velocity with depth and time. Initially the magma column is under very high pressure so that no gas is exsolved. The pressure decreases instantaneously and bubbles are allowed to grow in parts of the conduit where the melt is oversaturated. The pressure change affects every depth instantaneously.

The growth of the bubbles causes the magma to expand and this increase in volume is accommodated by accelerating the magma upwards from the nucleation depth where the bubbles first start to grow. Material extrudes and forms the equivalent of a spine or dome due to the high viscosity of the magma. For simplicity the magma in our model can escape freely from the top of the conduit so there is no additional pressure term to describe the effect of viscous magma flow. However, as a result of the growth of the spine with no erosion of the extruding material, the magmastatic pressure acting on a bubble will remain constant.

The pressure immediately after the decompression is the integrated weight of the magma above this depth:

$$P(z) = P_{ex} + \int_0^z g\,\rho(\xi)\,d\xi \qquad (1)$$

where P_{ex} is the excess pressure, g is the acceleration due to gravity and $\rho(z)$ is the bulk density of the gas–liquid mixture. The depth z is measured downwards from the top of the spine where $z = 0$. Initially $\rho(z) = \rho_l$, the density of the melt, because there is no gas exsolved. The excess pressure is the result of loading on top of the conduit, either a preexisting lava dome or spine.

The solubility law gives the concentration C_i of gas at the bubble wall and approximates the minimum mass fraction of gas dissolved in the melt, m_g^d, at a depth z (Shaw, 1974):

$$C_i = K_H\sqrt{P(z)} \approx m_g^d \qquad (2)$$

where K_H, Henry's constant, is calibrated experimentally as 4.1×10^{-6} $\mathrm{Pa}^{-1/2}$ in a rhyolitic liquid with water as the only volatile in the system.

The maximum mass fraction of gas that can be exsolved, m_g^{MAX}, is given by (Papale, 1998):

$$m_g^{MAX} = \frac{m_g^t - m_g^d}{1 - m_g^d} \qquad (3)$$

where m_g^t is the total mass fraction of gas initially dissolved and is equivalent to the initial concentration of water in the melt C_m.

The growth of bubbles is not instantaneous. After the decompression there is an interval in which bubbles grow before the exsolved gas content adjusts to the change in pressure. The bubble growth can be described by a series of equations (Navon and Lyakhovsky, 1998) each describing a stage in the formation and growth of the bubble; first bubbles must nucleate, then they grow exponentially, a result of the high surface to volume ratio of the bubble. Later the growth is slower. Finally bubble growth stops when the gas mass fraction that is out of solution equals m_g^{MAX}.

Immediately after the decompression event the supersaturation pressure ΔP at each depth can be calculated using (Lyakhovsky et al., 1996):

$$\Delta P = \left(\frac{m_g^t}{K_H}\right)^2 - P(z) \qquad (4)$$

If ΔP is positive, gas will be available to come out of solution and diffusion will take place until the amount of gas still dissolved reaches the amount given by the solubility law (Eq. 2).

The critical radius of the bubble r_{CR} is at an unstable equilibrium. If the bubble formed has a radius smaller than the critical radius, capillary pressure will close the bubble. If a nucleus is formed with a radius greater than r_{CR}, then the bubble will start to expand. The critical radius is given by (Lyakhovsky et al., 1996):

$$r_{CR} = \frac{2\,\sigma}{\Delta P} \tag{5}$$

where σ is the surface tension. Since ΔP depends on depth (Eq. 4), the critical radius becomes larger with increasing depth and decreasing oversaturation. A small bubble has a high surface area to volume ratio making diffusion very rapid. This is described by an exponential law (Lyakhovsky et al., 1996):

$$r = r_{CR} + (r_0 - r_{CR})\exp\left(\frac{\Delta P\, t}{4\,\eta}\right) \tag{6}$$

where r is the radius at a time t after nucleation, r_0 is the initial size of the bubble, set to $1.01 \times r_{CR}$ (Navon and Lyakhovsky, 1998), and η is the viscosity of the melt. At longer time periods bubble growth is described by a square root law (Lyakhovsky et al., 1996):

$$r^2 = \frac{2\,D\,\rho_l(C_m - C_i)}{\rho_g}t - \frac{2}{3}\frac{D\,\eta}{P}\frac{\rho_l}{\rho_g}(2C_m + C_i)\,log\left(\frac{\Delta P}{\eta}t\right) \tag{7}$$

where D is the diffusivity, ρ_g is the density of the gas and ρ_l is the density of the melt. The transition between the two curves occurs at the time when they cross.

For any time t it is possible to calculate the radius of a bubble at a depth z. The volume of gas, V_g produced by 1 m^3 of melt is given by:

$$V_g = \frac{4}{3}\pi r^3 N \tag{8}$$

where N is the bubble number density at the time of nucleation. Once the bubbles start to grow, the total volume of the magma increases and the number density of bubbles relative to the volume of magma will decrease if no new bubbles nucleate. Relative to the melt the number density is constant. The volume fraction of gas v_g will be:

$$v_g = \frac{V_g}{\left(1 - \frac{V_g \rho_g}{\rho_l}\right) + V_g} \tag{9}$$

where the term in parentheses is the volume of melt left after the bubbles have grown. This term conserves mass. The density of gas within the bubbles is given by:

$$\rho_g(z) = \frac{M_{H_2O}\,P(z)}{R\,T} \tag{10}$$

where M_{H_2O} is the molecular mass of water, T is the temperature of the magma in Kelvin and R is the gas constant. This assumes an ideal gas and equilibrium between pressure inside the bubble and magmastatic pressure.

The density ρ of the mixture is given by:

$$\rho = (1 - v_g)\,\rho_l + v_g\,\rho_g(z) \tag{11}$$

The mass fraction of gas exsolved is given by (Neuberg, 2000):

$$m_g^e = \frac{\rho_g}{\rho}v_g \tag{12}$$

If just one bubble were to nucleate, it would continue to grow, if very slowly, forever. In a magma containing many bubbles, growth will stop as the concentration of residual water dissolved in the melt approaches m_g^d (given by Eq. 2). The equations are only applied until $m_g^e = m_g^{MAX}$ at which point bubble growth stops and the mass fraction of gas exsolved remains constant at m_g^{MAX}. Then the density of the mixture is given by:

$$\frac{1}{\rho(z)} = \frac{1 - m_g^{MAX}}{\rho_l} + \frac{m_g^{MAX}}{\rho_g(z)} \tag{13}$$

If this value for the equilibrium density and m_g^{MAX} are substituted into Eq. 12, the volume fraction of gas exsolved is obtained when equilibrium is reached.

The seismic velocity, α, in a gas-liquid mixture is derived by Neuberg and O'Gorman (2002) as:

$$\alpha = \frac{1}{\sqrt{\frac{(1 - v_g)\rho}{B_l} + \frac{v_g\rho}{P}}} \tag{14}$$

where v_g is the volume fraction of gas and B_l is the bulk modulus of the liquid. The bulk modulus of the liquid (incompressibility) is large compared with the pressure P, so the right hand term under the square root sign dominates as soon as any gas is exsolved.

The initial magmastatic pressure is used to calculate the volume of gas exsolved for a continuous depth profile. There is an increase in the total volume of the conduit and the extra volume created is piled up above the conduit. A new depth is calculated for any given initial depth which depends on the change of volume of the magma below that depth. In this way mass is conserved due to upward movement of magma in the conduit.

The model is now used to describe the behaviour of a system using appropriate values taken from the literature. The following parameters are used: the density of the melt is 2300 kg m^{-3} (Neu-

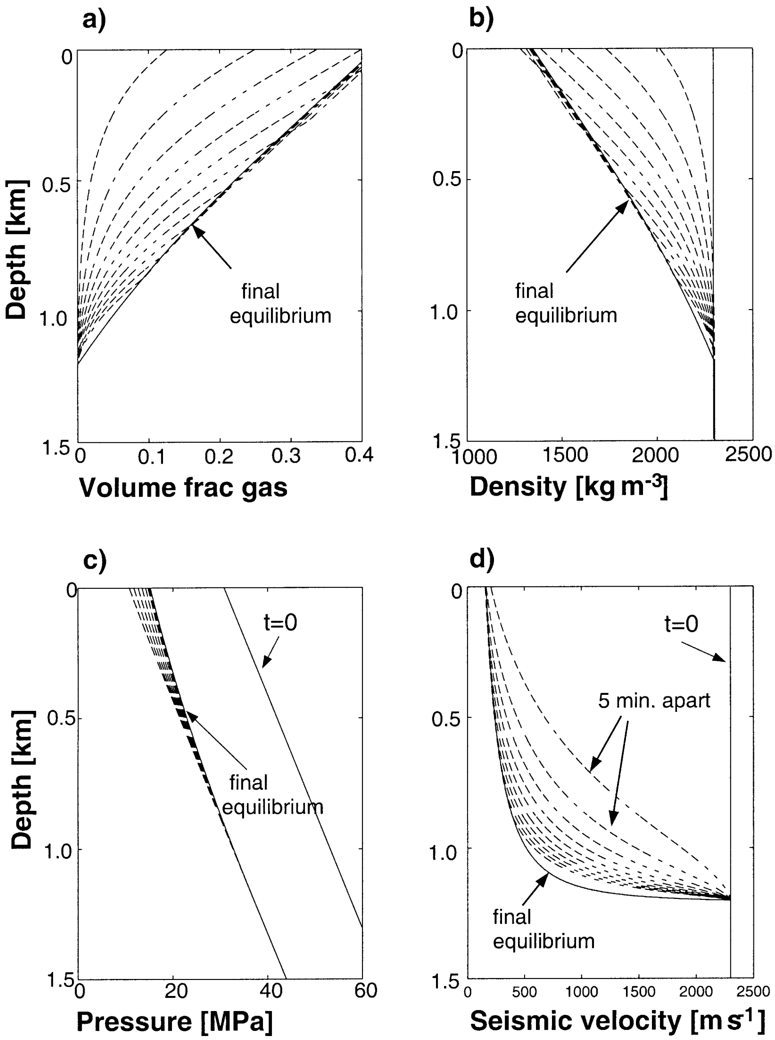

Fig. 1. Physical parameter profiles for the 'champagne bottle' model, with time, in a conduit after a large decompression event. Dotted lines are plotted at 5-min intervals and the solid line is the final equilibrium. Initially, there is no gas exsolved in the conduit so the density is 2300 kg m^{-3} at all depths, the pressure is greater than 28 MPa at the surface and increases linearly with depth and the seismic velocity is 2300 m s^{-1} at all depths. These initial conditions at $t=0$ are marked with a solid line.

berg, 2000) and the seismic velocity of the melt is 2300 m s^{-1} (Rivers and Carmichael, 1987). This gives the melt a bulk modulus of 1.21×10^{10} Pa s. The temperature of the melt is 1120 K (Devine et al., 1998). The diffusivity and the surface tension are 3×10^{-11} m^2 s^{-1} (Lyakhovsky et al., 1996) and 0.05 N m^{-1} (Lyakhovsky et al., 1996), respectively. The mass fraction of water initially dissolved in the melt is 2.5 wt% resulting in a viscosity of 10^6 Pa s (Spera, 2000). A bubble number density of 10^{10} is used which is within the range of number densities observed in nucleation experiments (Navon and Lyakhovsky, 1998). This value is much smaller than the typical values of 10^{14}–10^{16} in silicic pumice (Cashman et al., 2000).

Fig. 1 shows how the volume fractions of gas, density, pressure and seismic velocity evolve with time after a decompression event. The initial excess pressure before the decompression is so high that all gas is completely dissolved at all depths in the conduit. After the decompression event excess pressure is assumed to be 10 MPa. Initially there is no gas exsolved anywhere in the conduit, so the density and seismic velocities are constant for the melt at all depths. The dotted lines are plotted at 5-min intervals and the solid line is the equilibrium solution reached when $t \to \infty$. The final excess pressure acting on the system when equilibrium is reached is 15.2 MPa. This pressure increase is the result of the extruded lava piled up on top of the conduit as a dome or spine.

The bubbles grow, increasing the volume fraction of gas until a new equilibrium is reached. Then the bubbles stop growing (Fig. 1a). The bubbles grow more rapidly higher in the conduit and reach equilibrium in a shorter time despite having to reach a greater size.

Once the bubbles stop growing there is a decrease in the volume fraction of gas exsolved at any given depth and this decrease continues until equilibrium has been reached at all depths. This decrease is not caused by bubbles becoming smaller but by the upward motion of the magma in the conduit as the bubbles expand. Then smaller bubbles from greater depths ascend taking the place of the larger bubbles which have in turn moved further up the conduit.

The density of the magma decreases with the increasing gas content (Fig. 1b). The maximum value of density is 2300 kg m^{-3} when no gas is exsolved. At the top of the conduit the final density is 1300 kg m^{-3}. Lower in the conduit the difference between the initial and final densities is not as big because less gas has been exsolved.

After an initial large decrease the pressure increases gradually with time as the extruded lava piles up on top of the conduit (Fig. 1c). This change is small at the top of the conduit, increasing by 5.2 MPa, since only a small volume of melt has been extruded. The pressure only changes in parts of the conduit where bubbles have grown. Below the nucleation depth there is no change in pressure at any depth because there is still the same weight of magma resting on top.

The seismic velocity decreases with time as gas exsolves (Fig. 1d). It also increases with depth reflecting the increasing pressure which holds the gas in solution. The seismic velocity decreases very rapidly as soon as bubbles form (Eq. 14) and once the volume fraction of gas exceeds 0.1, seismic velocities are as small as 100–500 m s^{-1}. This means the velocity remains small after an initial rapid decrease. At the top of the conduit the velocity decreases almost to the equilibrium value in the first five minutes after decompression because the gas exsolves very rapidly. Lower in the conduit the equilibrium solution is reached more slowly. The decrease in seismic velocity at the nucleation level becomes more dramatic with time and eventually reaches the equilibrium value.

Fig. 2 shows the volume fraction of gas, density, pressure and seismic velocity as a function of time for two depths, 0.5 km and 1 km. At 0.5 km the bubbles grow more rapidly because of the larger supersaturation and so the volume fraction of gas correspondingly increases more rapidly. More gas is exsolved at 0.5 km than at 1 km because the pressure is lower. The density decreases gradually with time at both depths reflecting the increasing volume of gas. The pressure increases due to material piling up. The seismic velocity at 0.5 km decreases dramatically until 500 s and then only decreases gradually as the remainder of the gas is exsolved. At 1 km the change is more gentle because the volume of gas is much smaller.

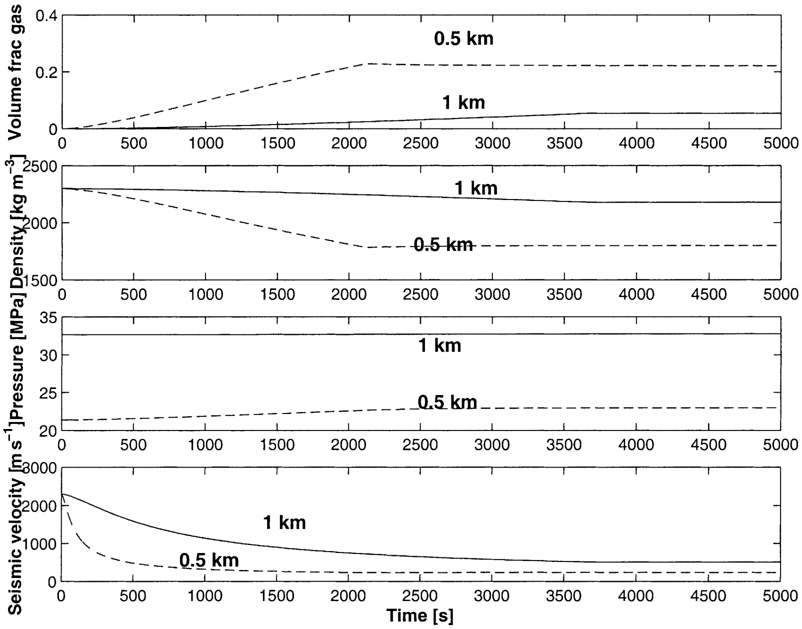

Fig. 2. Physical parameters plotted with respect to time for depths of 0.5 km (dotted line) and 1 km (solid line) for the 'champagne bottle' model.

The method described in this paper converges on the same equilibrium conditions as the melt-bubble equilibrium described by Neuberg and O'Gorman (2002), where an iterative approach is used: starting with the magmastatic pressure, the equilibrium gas content and densities are calculated as a function of depth. These are then used to determine a new pressure profile. These steps are repeated until the system converges. The iterative approach by Neuberg and O'Gorman (2002) is replaced in the present method by the evolution of the magma properties with time.

2.2. Dome collapse

The 'champagne bottle' model allows us to examine the effect of increasing bubble size on seismic velocity and density. However, a very large initial pressure is required to keep all the water in solution. For a water concentration of 2.5 wt% all the water is in solution at pressures greater than 28 MPa. This pressure corresponds to a magma column of 1.3 km height, the sudden removal of which presents an unlikely scenario.

Smaller dome collapses are more common and a collapse of, for example, 200 m would result in a decrease in the excess pressure of 4–5 MPa. If the initial pressure is 20 MPa, then the conduit will already contain some bubbles which will grow after the decompression event. If the melt becomes supersaturated, new bubbles will nucleate and grow below the initial vesiculation level. Again, as the concentration of gas in the melt reaches equilibrium at the new pressure, bubble growth will decrease and stop.

Using this initial condition we have recalculated the model. The initial conditions before the decompression are found using the method of Neuberg and O'Gorman (2002) and are set up for the required initial pressure. The exsolved gas is distributed so that the bubble number density, N, is constant throughout the conduit. After the decompression, the bubbles nucleate and grow below the nucleation depth for the initial pressure, as described using Eqs. 4–8. Above this depth the equations describing the growth of the bubble must be modified so that they describe the growth of a bubble with initial radius $r = r(z) \neq 0$.

At depths where bubbles are already present, the supersaturation pressure ΔP is redefined as:

$$\Delta P = P_{t_0}(z) - P_t(z) \tag{15}$$

where $P_{t_0}(z)$ and $P_t(z)$ are the pressure at a given depth z before and after the decompression event, respectively. The supersaturation pressure is smaller when there are already bubbles present because the initial concentration of water in the melt is lower.

Again the initial growth of the bubbles is exponential and is described by the equation (Lensky et al., 2002):

$$r = r_0 \exp\left(\frac{\Delta P\, t}{4\,\mu}\right) \tag{16}$$

where r_0 is the initial radius. At longer times we use the following approximation:

$$r^2 = r_0^2 + \frac{2\,D\,\rho_l(C_m(z) - C_i)}{\rho_g} t \tag{17}$$

where $C_m(z)$ is the concentration of gas in the melt before decompression. $C_m(z)$ is depth-dependent because it depends on the initial mass frac-

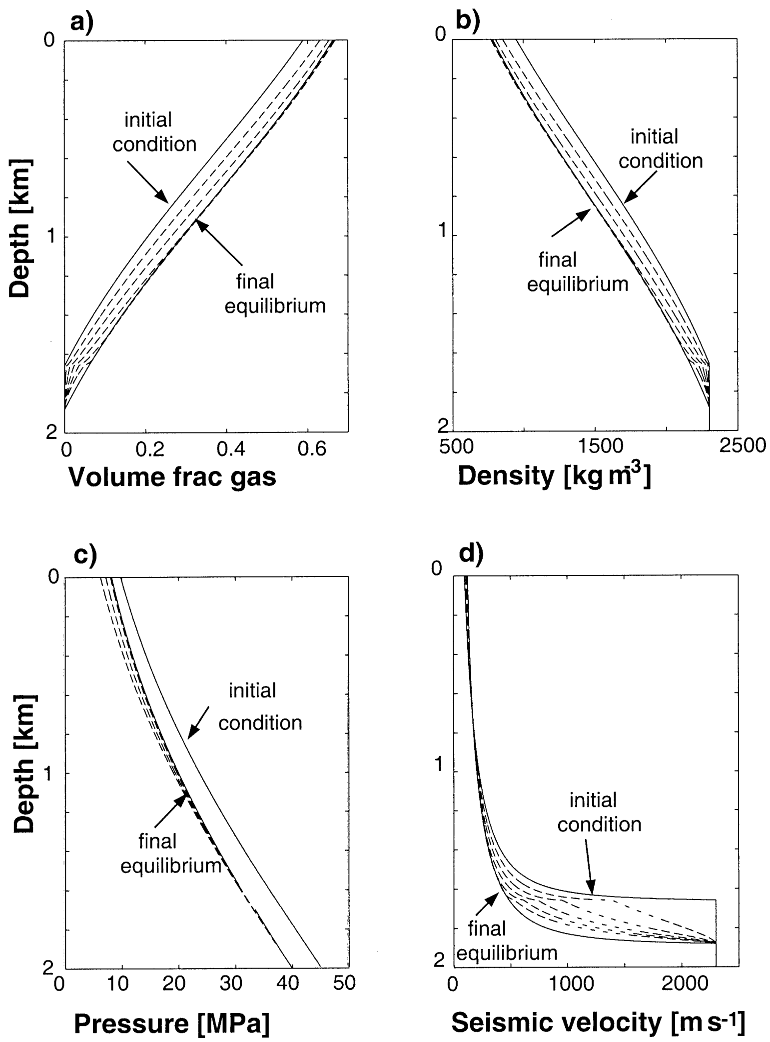

Fig. 3. Physical parameter profiles for the 'dome collapse' model, with time, in a conduit after a decompression event from 10 to 5 MPa. The initial equilibrium at 10 MPa is plotted with a solid line, dotted lines are plotted at 10-min intervals after decompression, and the final equilibrium at lower pressure is also plotted as a solid line.

tion of gas exsolved at each depth. Once the bubble radius has been calculated the method for obtaining the volume of exsolved gas, density and seismic velocity of the magma is the same as for the previous model (Eqs. 9–14).

Fig. 3 shows the result for a pressure decrease from 10 to 5 mMPa. All other parameters are the same as for the 'champagne bottle' model. The initial conditions are plotted. The parameters are then plotted at 10-min time intervals, and for the final equilibrium. Once the bubbles have stopped growing, the final pressure acting at the top of the conduit is 8.2 MPa. Again, the increase is the result of extruded magma piled on top of the conduit.

The volume fraction of exsolved gas increases with time before the system reaches equilibrium (Fig. 3a). The nucleation depth increases by 200 m. The bubbles between the initial and final nucleation depths form after the decompression event and grow according to Eqs. 4 and 7. As in the 'champagne bottle' model, bubble growth is initially more rapid, slowing with time as equilibrium is reached. Above the initial nucleation depth the change in volume is much smaller because there is already some exsolved gas and equilibrium is reached more rapidly because the bubbles do not have to grow as much. Below the initial nucleation depth equilibrium is reached more slowly.

The density decreases with time (Fig. 3b), consistent with the increasing volume of gas. The change in the densities before and after the decompression are not as big as for the 'champagne bottle' model because gas is already exsolved.

Initially the pressure decreases sharply by

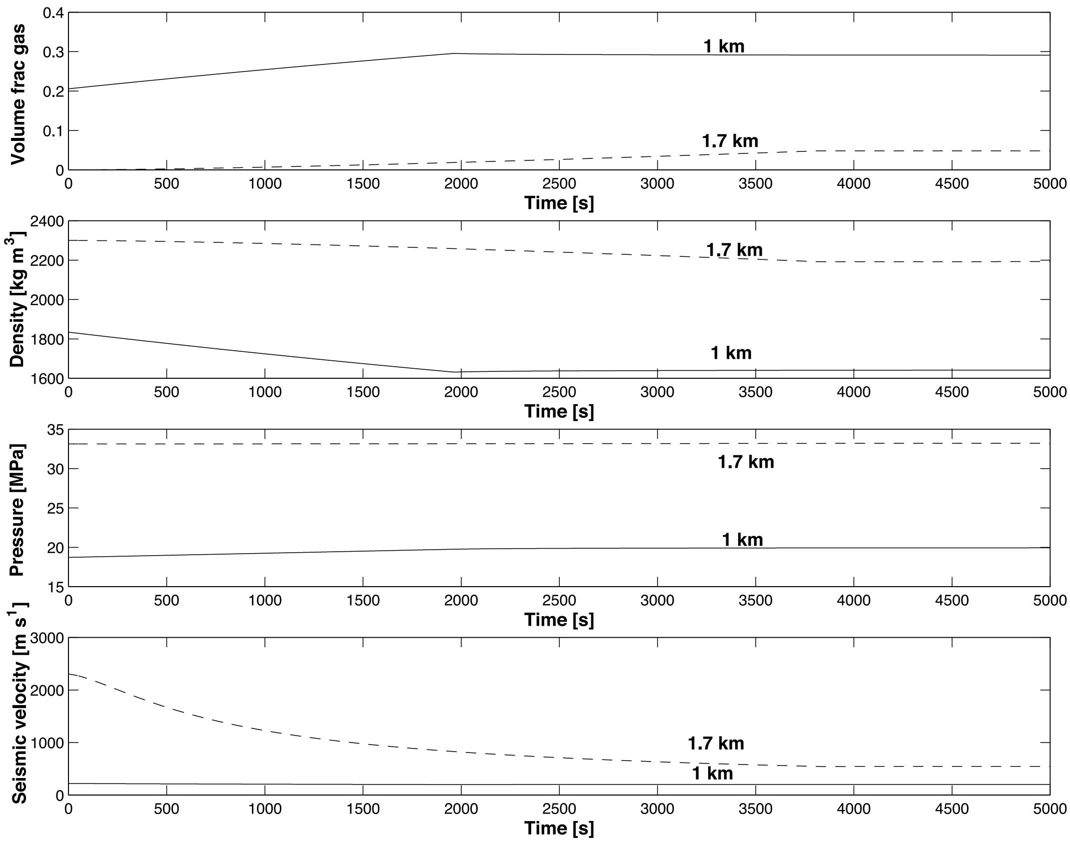

Fig. 4. Physical parameters plotted with respect to time for depths of 1 km (solid line) and 1.7 km (dotted line) for the 'dome collapse' model.

5 MPa at all depths (Fig. 3d), as a result of the decompression event. It then increases steadily as extra material is extruded until equilibrium is reached at all depths. The increase in pressure is not as big as for the 'champagne bottle' model because the change in volume is smaller.

Above 1 km depth there is no substantial change in the seismic velocity (Fig. 3d) because there is already a large volume of exsolved gas. Below this depth the effects of the increased bubble size are more noticeable. The seismic velocity decreases down to the new nucleation level. At first the decrease in seismic velocity is large immediately below the initial nucleation level. The bubbles grow faster here than deeper in the conduit because the oversaturation is higher. This is the same as the trend in the previous model where the decrease at the top of the conduit was large immediately after the decompression event. At the nucleation depth the seismic velocity continues to fall until the new equilibrium is reached.

Fig. 4 shows the volume fraction of gas, density, pressure and seismic velocity against time for depths of 1 km and 1.7 km. At 1 km bubbles are present before the decompression and these start to grow. The volume of gas increases from the initial value. The density decreases as the gas is exsolved but the seismic velocity remains almost constant. At 1.7 km there are no bubbles present before the decompression event so the volume of gas increases from zero. The seismic velocity decreases from the initial value of 2400 m s^{-1}.

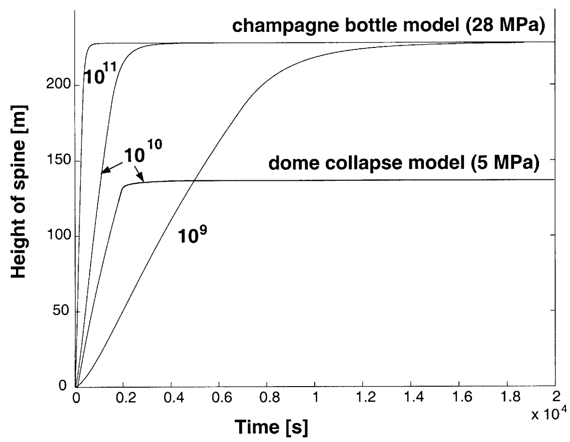

Fig. 5. The effect of bubble number density on the growth rate of the spine.

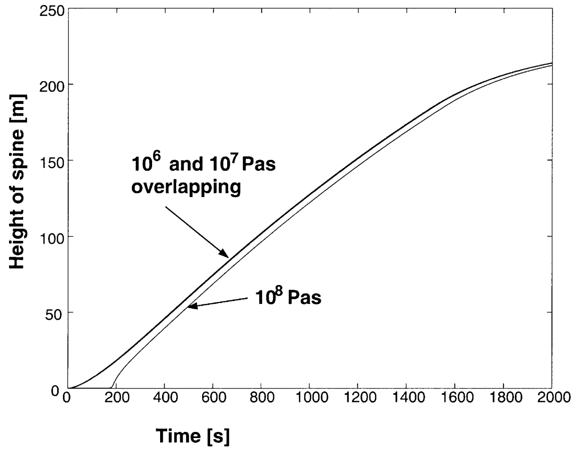

Fig. 6. The effect of viscosity on the growth rate of the spine.

3. Effects of model parameters

In the following we identify the parameters which control the rate of bubble growth and therefore the timescale for the gliding lines in the seismic spectra. The frequencies of the seismic events depend on the seismic velocity and nucleation depth in the conduit and the timescales with which these parameters change is important. The growth of the spine indicates the rate at which the volume of gas in the conduit changes and is used to illustrate changes in the rate of bubble growth and therefore the rates of change of the seismic parameters. The height of the extruded spine is shown as a function of time in Figs. 5 and 6 and can be used for an initial comparison with observations.

The spine is magma extruded to accommodate the extra volume created by the growth of the bubbles. It is extruded from the top of the conduit so it is a gas/melt mixture. However, in the figures the volume of gas is excluded and just the volume of extruded melt is plotted. This is to simulate the extrusion of a dense spine where the gas has already escaped as is seen at volcanoes including Montserrat and Mount Pelée (Lacroix, 1904). The time dependence of the degassing is not modelled and the magma can escape freely from the top of the conduit, so the spine growth is not modelled accurately. The height of the spine is shown rather than the volume extruded, because the volume is the height multiplied by the cross sectional area of the conduit. The area is constant as expansion is only allowed vertically. If the height is plotted the results apply to a conduit of any diameter.

3.1. Effect of bubble number density

To examine the effect of the number density of nucleated bubbles, simulations were run with initial number densities of 10^9 m^{-3}, 10^{10} m^{-3} and 10^{11} m^{-3}. The initial values of the other parameters are the same as for the 'champagne bottle' model and kept constant for each simulation. The results for the 'champagne bottle' model with a nucleation number density of 10^{10} mm^{-3} are identical to those plotted in Fig. 1.

Fig. 5 shows the effect of different number density of bubbles on the growth of the spine. Each simulation shows the same pattern of growth: initial rapid growth of the spine as bubbles grow at all depths in the conduit, followed by a slower extrusion as equilibrium is reached deeper in the conduit. Finally, growth of the spine ceases when equilibrium is reached at all depths and there is no further bubble growth.

When the number density of bubbles increases, the initial growth of the spine is more rapid and equilibrium is reached more quickly. For the 'champagne bottle' model all the spines reach the same final height because the final gas concentrations are identical. The rate at which the bubbles grow is the same for different number densities, but the rate at which the volume of exsolved gas grows increases with the number of bubbles. Thus the equilibrium concentration is reached more rapidly.

Fig. 5 also shows the results for the height of the spine as a function of time for the 'dome collapse' model simulated in figure dome. For a decompression of only 5 MPa the final height of the spine is less than that for the 'champagne bottle' model because with a smaller decompression not as much gas comes out of solution.

If the results are compared with those for the 'champagne bottle' model with the same number density of bubbles, the timescales for the growth of the spine are very similar. In both cases the spines stop growing after 4000 s. For different sizes of decompression events the time for reequilibration is very similar if all other parameters are kept the same. The transition from rapid to slow growth of the spine is more gradual for the 'champagne bottle' model. This is because for the 'dome collapse' model the supersaturation after decompression is a constant up to the initial equilibrium depth, so equilibrium is reached almost simultaneously at all depths in the conduit. Until this time there is rapid growth of bubbles throughout the conduit. After this there is only growth below the initial equilibrium depth and the volume change is very small, so the spine grows much more slowly. For the 'champagne bottle' model the supersaturation decreases gradually with depth, so equilibrium is reached gradually with depth and the transition is smoother. Bubble number density controls the time it takes after decompression before the new equilibrium is reached.

3.2. Effect of viscosity

Fig. 6 shows the effect of melt viscosity on the growth of the spine, all other parameters being kept constant. Viscosity is very dependent on the concentration of water in the melt and the viscosity of rhyolite at 900°C can be as high as 10^8 Pa s if the water concentration is less than 0.1 wt% (Shaw, 1972; Hess and Dingwell, 1996).

A change in the viscosity does not change the equilibrium concentration so the final size of the bubbles is the same. Viscosity is important when the bubbles are small and can delay bubble growth as discussed by Sahagian et al. (1994) and Sparks (1994). For a very high viscosity of 10^8 Pa s this time delay can be seen clearly: bubble growth is delayed by almost 200 s. However, for viscosities of 10^6 and 10^7 Pa s the time delay is small. Over long timescales the results look very similar and the viscosity does not have a large effect.

4. Limitations of the model

The solutions for bubble growth adopted in this paper are too simplified to fully describe the physical system. Lyakhovsky et al. (1996) derive Eq. 7 as an analytical solution describing bubble growth when $t \to \infty$ if the supersaturation is assumed to be constant. With a high number density of bubbles the concentration of water remaining in the melt decreases with time, leading to a decrease in the supersaturation. The bubble would therefore grow more slowly at longer time periods than described by the equation.

Lensky et al. (2002) show that the analytical solution is a good approximation to the numerical solution when $t < \tau_d$ where τ_d is the viscous timescale:

$$\tau_d = \frac{1}{D}\left(\frac{3}{4\pi N}\right)^{\frac{2}{3}} \tag{18}$$

For a number density of 10^{10} m^{-3} the viscous timescale is 2700 s. In the calculations the bubbles stopped growing after 3800 s, so only during the last 1000 s would the growth be slower. For a number density of 10^9 m^{-3} and 10^{11} m^{-3} the viscous timescale is 13 000 s and 600 s, respectively. The viscous timescale is approximately 70% of the total time in which the bubbles grow. After this the solutions will overestimate the amount of exsolved gas and equilibrium is reached more rapidly and the bubbles should be modelled with a time-dependent supersaturation.

The growth of the spine is used to illustrate how rapidly the bubbles are growing. For a number density of 10^{10} m^{-3}, the spine grew 210 mm in 35 min. This number is hard to compare with observations; at Montserrat it is rare that visibility is good enough to measure the growth, and erosion of the spine material is continuous. However, the growth rate obtained from the model is probably more rapid than in reality. Modelling the spine growth accurately is beyond the scope of our model because no flow dynamics of the extruding magma are included. The extra material can escape freely. However, this frictionless escape is partly compensated by keeping the bubble number density low.

5. Conclusions

We can model profiles of physical parameters in a magma filled conduit to obtain a time history for the re-equilibration of the system after a decompression event. For both the 'champagne bottle' model and the 'dome collapse' model the volume fraction of exsolved gas increases after a decompression event resulting in a change in the profiles of the density and the seismic velocity. The density decreases significantly throughout the conduit in both models. The 'champagne bottle' model has a large decrease in the seismic velocity throughout the conduit. In the 'dome collapse' model, the nucleation level moves downward and the part of the conduit with slow seismic velocities extends to greater depths. Where bubbles were already present, above the initial nucleation level, the seismic velocities are almost unchanged.

Timescales derived from these models are similar to those observed for gliding lines. At Montserrat they occur over a 30-min period (Neuberg et al., 2000), corresponding to the timescale for a bubble number density of 10^{10}. The timescale is the same for the 'champagne bottle' model and the 'dome collapse' model, so the initial conditions are not very important.

Viscosity is an important factor. It can delay the onset of the changes in frequency. However, after a dome collapse seismic signals may be dominated by signals from pyroclastic flows and the gliding spectral lines cannot be observed until after the pyroclastic flows run out. The small time delay would go unnoticed.

Acknowledgements

This work was funded by NERC through Ph.D. Grant No. GT 04/99/ES/117 and by MULTIMO (EVGI-CT-2000–0002) which is supported by the Environmental and Sustainable Development Program of the European Commission Research Directorate General. Thanks are due to P. Jousset, A. Jolly, and especially N. Lensky for helpful discussions. The authors are indebted also to M. Felix for support and reading the first drafts. We are grateful for the assistance given by the staff at the Montserrat Volcano Observatory. Reviews by M. Hellweg and an anonymous reviewer improved the final manuscript considerably.

References

Benoit, J., McNutt, S., 1997. New constraints on source processes of volcanic tremor at Arenal Volcano, Costa Rica, using broadband seismic data. Geophys. Res. Lett. 24, 449–452.

Biot, M.A., 1952. Propagation of elastic wave in a cylindrical bore. J. Appl. Phys. 42, 82–92.

Cashman, K.V., Sturtevant, B., Papale, P., Navon, O., 2000. Magmatic fragmantation. In: Encyclopedia of Volcanoes. Academic Press, New York, pp. 421–40.

Chouet, B.A., 1986. Dynamics of a fluid-driven crack in three dimensions by the finite difference method. J. Geophys. Res. 91, 13967–13992.

Devine, J.D., Murphy, M.D., Rutherford, M.J., Barclay, J., Sparks, R.S.J., Carroll, M.R., Young, S.R., Gardner, J.C., 1998. Petrological evidence for pre-eruptive pressure–temperature conditions and recent reheating of andesitic magma erupting at Soufrière Hills Volcano, Montserrat, WI. J. Geophys. Res. 25, 3669–3672.

Fehler, M.C., 1983. Observations of volcanic tremor at Mount St Helens volcano. J. Geophys. Res. 88, 3476–3484.

Ferrazzini, V., Aki, K., 1987. Slow waves trapped in a fluid-filled crack: Implications for volcanic tremor. J. Geophys. Res. 92, 9215–9223.

Hess, K.-U., Dingwell, D.B., 1996. Viscosities of hydrous leucogranitic melts: A non-Arrhenian model. Am. Mineral. 81, 1297–1300.

Lacroix, A., 1904. La montagne Pelée et ses éruptions. Masson, Paris.

Lensky, N., Lyakhovsky, V., Navon, O., 2002. Expansion dynamics of volatile-supersaturated fluid and bulk viscosity of bubbly magmas. Earth Planet. Sci. Lett. (in press).

Lyakhovsky, V., Hurwitz, S., Navon, O., 1996. Bubble growth in rhyolitic melts: Experimental and numerical investigation. Bull. Volcanol. 58, 19–32.

Navon, O., Lyakhovsky, V., 1998. Vesiculation processes in silicic magmas. In: Gilbert, J.S., Sparks, R.S.J. (Eds.), The Physics of Explosive Volcanic Eruptions 145. Geological Society, London, Special Publications, pp. 27–50.

Neuberg, J., 2000. Characteristics and causes of shallow seismicity in andesitic volcanoes. Philos. Trans. R. Soc. Lond. (A) 358, 1533–1546.

Neuberg, J., Baptie, B., Luckett, R., Stewart, R., 1998. Results from the broadband seismic network on Montserrat. Geophys. Res. Lett. 25, 3661–3664.

Neuberg, J., Luckett, R., Baptie, B., Olsen, K., 2000. Models of tremor and low-frequency earthquake swarms on Montserrat. J. Volcanol. Geotherm. Res. 101, 83–104.

Neuberg, J., O'Gorman, C., 2002. A model of the seismic wavefield in gas-charged magma: Application to the Soufriére Hills Volcano, Montserrat. In: Druitt, T.H., Kolelaar, B.P. (Eds.), The Eruption of the Soufrière Hills Volcano, Montserrat, from 1995 to 1999. Memoirs Geological Society, London, pp. 603–609.

Papale, P., 1998. Volcanic conduit dynamics. In: Freundt, A., Rosi, M. (Eds.), From Magma to Tephra. Elsevier, Amsterdam, pp. 55–89.

Powell, T., Neuberg, J., 2002. Time dependent features in tremor spectra. J. Volcanol. Geotherm. Res. (in press).

Proussevitch, A.A., Sahagian, D.L., 1996. Dynamics of coupled decompressive bubble growth in magmatic systems. J. Geophys. Res. 101, 17447–17455.

Proussevitch, A.A., Sahagian, D.L., Anderson, A.T., 1993. Dynamics or diffusive bubble growth in magmas: Isothermal case. J. Geophys. Res. 98, 22283–22307.

Rivers, M.L., Carmichael, I.S.E., 1987. Ultrasonic studies of silicate melts. J. Geophys. Res. 92, 9247–9270.

Sahagian, D.L., Proussevitch, A.A., Anderson, A.T., 1994. Reply. J. Geophys. Res. 99, 17829–17832.

Schlindwein, V., Wassermann, J., Scherbaum, F., 1995. Spectral analysis of harmonic tremor signals at Mt. Semeru volcano, Indonesia. Geophys. Res. Lett. 22, 1685–1688.

Shaw, H.R., 1972. Viscosities in magmatic silicate liquids: an empirical method of prediction. Am. J. Sci. 272, 870–893.

Shaw, H.R., 1974. Diffusion of H_2O in granitic liquids, Part 1. Experimental data. In: Hofmann, A.W., Giletti, B.J., Yoder, H.S., Yund, R.A. (Eds.), Geochemical Transport and Kinetics. Carnegie Institution of Washington, pp. 139–172.

Sparks, R.S.J., 1994. Comment on 'Dynamics of diffusive bubble growth in magmas: Isothermal case' by A.A. Prossevitch, D.L. Sahagian and A.T. Anderson. J. Geophys. Res. 99, 17827–17828.

Spera, F.J., 2000. Physical properties of magmas. In: Encyclopedia of Volcanoes. Academic Press, New York, pp. 171–190.

Voight, B., Hoblitt, R.P., Clarke, A.B., Lockhart, A.B., Miller, A.D., Lynch, L., McMahon, J., 1998. Remarkable cyclic ground deformation monitered in real-time on Montserrat and its use in eruption forcasting. Geophys. Res. Lett. 25, 3405–3408.